Degradation study of tris(2-butoxyethyl) phosphate with TiO_2 immobilized on aluminum meshes employing artificial neural networks

Ramon Vinícius Santos de Aquino, Ada Azevedo Barbosa, Rafaela Ferreira de Carvalho, Marina Gomes Silva, Welenilton José do Nascimento Júnior, Túlio Diego da Silva, Josivan Pedro Silva and Otidene Rossiter Sá da Rocha

ABSTRACT

This work presents the study of tris(2-butoxyethyl) phosphate advanced oxidation in TiO_2-containing systems. Titania was immobilized on aluminum surfaces from recyclable materials and the results were compared with the suspension system. The initial concentration of photocatalyst and the oxidizing agent was optimized in a 2^3 experimental design and a kinetic study of the reactions was performed in the selected conditions. The experimental data were fitted to the pseudo-first-order model (rate constants estimated at 0.0129 ± 0.0009 and 0.0079 ± 0.0006 min^{-1} for the systems with TiO_2 in suspension and immobilized, respectively). Artificial neural networks were also employed to model the experimental data and they presented correlation coefficients superior to 0.98 in all the training operations. After five cycles of degradation, the TiO_2–aluminum meshes exhibited a very low decrease in photocatalytic activity (inferior to 2%). Acute phytotoxicity assays demonstrated that the byproducts of the oxidation of TBEP molecules are less toxic than the raw samples regarding lettuce seeds. For both TiO_2 systems, COD decreased considerably as a consequence of the degradation. The immobilized TiO_2 system achieved similar degradation rates when compared with the suspension system.

Key words | aluminum supports, artificial neural networks, immobilized titania, photocatalytic degradation, tris(2-butoxyethyl) phosphate

Ramon Vinícius Santos de Aquino
Ada Azevedo Barbosa
Rafaela Ferreira de Carvalho
Marina Gomes Silva
Welenilton José do Nascimento Júnior
Josivan Pedro Silva
Otidene Rossiter Sá da Rocha (corresponding author)
Department of Chemical Engineering,
Universidade Federal de Pernambuco (UFPE),
Prof. Arthur de Sá av., Cidade Universitária, Recife,
Brazil
E-mail: *otidene.rocha@ufpe.br*

Túlio Diego da Silva
Centro de Tecnologias Estratégicas do Nordeste (CETENE),
Av. Prof. Luís Freire, 1, Cidade Universitária, Recife, PE, 50740-545,
Brazil

INTRODUCTION

Organophosphate esters (OPEs) are widely employed in coating rubber, polymeric materials, textiles, metal products and packaging as flame retardants. OPEs can contaminate the environment by leaching, abrasion and volatilization mechanisms, turning into recalcitrant species (Greaves *et al.* 2016; Vykoukalová *et al.* 2017). Many of the chemicals from this class are known to cause adverse effects to water ecosystems and human health due to carcinogenic, mutagenic and neurotoxic properties. Among these compounds, it is worth highlighting tris(2-butoxyethyl) phosphate (TBEP), tributyl phosphate (TBP) and tris(2-chloroethyl) phosphate (TCEP), which present huge levels of toxicity even at very low concentrations (Greaves *et al.* 2016).

Physical, chemical and biological conventional methods have been demonstrated to be inefficient in the removal of OPEs in wastewater because these pollutants are highly stable, and therefore, require the search for alternative techniques for their treatment (Charamba *et al.* 2018). Advanced oxidation processes (AOPs) are considered an alternative to treating non-biodegradable organic chemicals, acting non-selectively, reaching high degradation rates and in most of the cases, forming less harmful by-products (Nascimento Júnior *et al.* 2018).

However, when mineralization is not achieved, a range of by-products may be formed and among them, more harmful species than the parent chemicals. For this reason,

doi: 10.2166/wst.2019.363

biotoxicity assays using living organisms are suggested in order to evaluate comparatively the acute toxicity of treated AOP samples regarding the raw samples (Utzig *et al.* 2019).

AOP methods target the complete or partial mineralization of organic compounds from the generation of free radicals with high oxidant potential (Nasirian *et al.* 2017). In heterogeneous photocatalysis, titanium dioxide (TiO_2) is the most employed photocatalyst due to its high performance, low toxicity and low cost (Barbosa *et al.* 2019). As a semiconductor, titania is excited by a radiation equal or of superior energy to its band-gap, generating an electron–hole pair able to oxidize water molecules and generate free radical species with high oxidation potential. Water and oxygen molecules can be adsorbed onto the surface of titania, interact chemically with the semiconductor and free radicals may be formed due to redox reactions (Wiedmer *et al.* 2016). The rutile phase of titania (3,2 eV) is able to absorb energy and form a hole in the UV electromagnetic spectrum from 200 to 380 nm (Bayarri *et al.* 2007).

Many reports in the literature dealing with TiO_2 in AOP processes operate directly with it in suspension since it is insoluble in water and some of them have achieved great results working with the powder immobilized on the surface of a range of materials, such as glass (Xing *et al.* 2018), ceramic (Veréb *et al.* 2014), chitosan (Huang *et al.* 2014) and polymers (Santos *et al.* 2018). These low-cost materials as supports make the catalytic systems more environmentally friendly and aim to reduce further costs of separation (Aquino *et al.* 2019). Aluminum is a metal that encompasses these characteristics, in addition to presenting suitable mechanical properties (Verran *et al.* 2005) to be a photocatalytic carrier and being a worldwide recyclable good.

One of the most promising techniques in modelling kinetic data is based on the use of artificial neural networks (ANNs). ANNs are able to predict the behavior of chemical processes even with no knowledge of the chemical routes (Barbosa *et al.* 2019). Nascimento Júnior *et al.* (2018) and Aquino *et al.* (2019) have implemented this method in predicting organic pollutant removal in AOP systems. The ANN learns the behavior trends of a particular process, including the chemical ones, and it does not require the comprehension of the chemical routes, which makes it feasible to evaluate complex reactions such as AOPs.

The present study deals with heterogeneous photocatalysis for the removal of TBEP flame retardant in suspended TiO_2 and immobilized over aluminium meshes manufactured from can seals. The novelty of the work relies on the usage of low-cost and mechanically resistant aluminum material, besides it being a product largely employed in recycling processes. Sample analyses were carried out by high-performance liquid chromatography (HPLC) and degradation kinetics was evaluated according to the pseudo-first-order (PFO) model and ANN method.

MATERIALS AND METHODS

TBEP ($C_{18}H_{39}O_7P$, 94%, purchased from Sigma Aldrich) samples were prepared at 1.0 mg/L in deionized water. Titanium dioxide (TiO_2-P25: 80% anatase, 20% rutile) employed in this study was acquired from Degussa Evonik Industries and hydrogen peroxide (30% v/v) was acquired from Solvay Peróxidos Brasil.

Manufacturing of aluminum meshes and TiO_2 immobilization

Aluminium meshes were manufactured from can rings obtained from commercial drinks. The meshes (8.0×4.5 cm, 1 mm depth) were calcined at 490 °C for 26 hours before the immobilization procedure. The immobilization of photocatalyst on aluminum surface was carried out as described by Barbosa *et al.* (2019). After immobilization of titania, the meshes were calcined once more for 2 hours at 490 °C in order to promote the adhesion of the photocatalyst particles.

Aluminum mesh characterization

The TiO_2-mesh was characterized by X-ray diffraction (XRD) and scanning electron microscopy (SEM). XRD used radiation of Cu Kα, 2 kVA power, 30 kV voltage and 30 mA current (XRD-600 Shimadzu diffractometer). The scanning was performed at 2θ between 20° and 80° at a pace of 0.02° and speed of $2°.s^{-1}$. Crystallographic letters were used to evaluate the characteristic peaks exhibited by the material (21-1272 and 21-1276 from International Center of Diffraction Data) and the data were compared with the raw aluminum material data. Morphology analyses of TiO_2-mesh were performed with samples before and after the thermal treatment (calcination) and immobilization procedure in a Tescan MIRA3 Microscope. Images at a magnification of 500× were accessed.

Analytical methods (HPLC-MS/MS)

TBEP samples were analysed by HPLC (Acquity, Waters, USA) coupled with a single quadrupole mass spectrometer (SQ Detector 2, Waters, EUA) equipped with an electrosprayer for ionization. The ionizing source operated at

3.5 kV of capillary voltage, 25 V cone voltage, and dewatering temperature of 150 °C and gas flow at a rate of 550 $L \cdot h^{-1}$. The TBEP raw sample (1.0 $mg \cdot L^{-1}$) was quantified according to its molecular weight (398.48 $g \cdot mol^{-1}$) by selected ion recording (SIR) mode.

Preliminary tests

The TBEP synthetic samples were treated in UVC, UVC/H_2O_2, UVC/$TiO_{2(suspended)}$, UV/$TiO_{2(immobilized)}$, UVC/H_2O_2/$TiO_{2(suspended)}$ and UVC/H_2O_2/$TiO_{2(immobilized)}$ systems. The treatment systems were also performed in the absence of radiation. The assays were carried out in cylindrical glass vessels (7.0 cm diameter and 5.5 cm height) inside a photoreactor in batch mode. The inner chamber of the reactor was coated with reflective material and the reactor contained a germicidal lamp (20 W, Tovalight T8, $\lambda =$ 253.7 nm). The samples underwent magnetic stirring during the operation and TiO_2-meshes were submerged in the reaction medium during the experiments.

Samples of 300 mL of TBEP (1.0 $mg \cdot L^{-1}$) were treated in each system for 240 minutes. Hydrogen peroxide was added at a concentration of 5.47 $mmol \cdot L^{-1}$ according to the stoichiometric balance of the degradation reaction between the pollutant and the oxidizing agent. The titania concentration at 500 $mg \cdot L^{-1}$ was based on the Santos *et al.* (2018) experiments. TBEP samples were brought into contact with TiO_2 under stirring in the preliminary systems for 30 minutes in order to reach adsorption equilibrium in the absence of the radiation source (Nasirian *et al.* 2017).

Experimental planning design

A 2^3 experimental design was performed to investigate the operational conditions in the selected UVC-based system from the preliminary tests. Concentration of TiO_2 (333.3, 500 and 666.7 $mg \cdot L^{-1}$), concentration of H_2O_2 (2.73, 5.47 and 8.20 $mmol \cdot L^{-1}$) and time (120, 180 and 240 minutes) were investigated. The central point was carried out in triplicate to determine the pure error of the experiment. Pareto charts were used to investigate the statistical significance of the parameters and their interaction in Statistica Experimental Design 6.0.

Kinetic study of TBEP degradation

The operational conditions were selected according to the experimental planning assays by the highest removal rates achieved. The experiments were carried out with TiO_2 in suspension and immobilized on aluminium meshes with eight sampling times for 360 minutes. The kinetic profiles were fitted to non-linear pseudo-first-order models in Origin Pro 9.0. Rate constants (k) and half-life reaction times ($t_{1/2}$) were estimated for both profiles.

ANNs were also employed to fit the experimental data provided by the UVC/H_2O_2/$TiO_{2(suspension)}$ and UVC/H_2O_2/$TiO_{2(immobilized)}$ systems. The software was developed in C# language in Unity 3D© according to Barbosa *et al.* (2019) and Göb *et al.* (1999). The software was able to receive input data, set a network type, run the training operation and display the resultant network in several forms. The network structure was 1:2:1, with time as the input variable, two neurons and concentration at time t as the output variable (response). The neural network was of type feed-forward with a sigmoidal function and all the data were normalized between −1 and 1 in the input in order to improve quality and speed of the networks. The performance of the network in describing a set of data could be evaluated by the mean absolute error and the correlation coefficient (R^2). Training times were estimated at around 2,600 seconds on a desktop computer.

Reuse of aluminum meshes

The reuse of TiO_2-meshes was evaluated in five consecutive cycles for 360 minutes in order to estimate the photocatalytic activity loss through the UVC/H_2O_2/$TiO_{2(immobilized)}$ system. Samples of 1.0 $mg \cdot L^{-1}$ of TBEP were applied in the degradation test cycles. The TiO_2-meshes were washed with distilled water and dried at 35 °C for 1 h at the end of each cycle. The temperature conditions were mild to not cause any change in the mesh structure and, consequently, alter the degradation efficiency.

Toxicity bioassays and water quality parameters

Phytotoxicity bioassays in *Lactuca sativa* (lettuce) seeds were adapted from Aquino *et al.* (2019) for raw TBEP samples and treated samples in the UVC/H_2O_2/$TiO_{2(suspension)}$ and UVC/H_2O_2/$TiO_{2(immobilized)}$ systems. Inhibition concentration of root growth for 50% of the organisms (IC_{50}) was calculated from the root elongation measurements. The relative growth index (RGI) was also estimated (Equation (1)):

$$RGI = \frac{ARS}{ARC} \quad (1)$$

where ARS represents the average root elongation in treated samples and ARC is the average root elongation in the negative control (deionized water).

Chemical oxygen demand (COD), pH and conductivity of raw and treated samples in the UVC/H_2O_2/$TiO_{2(suspension)}$ and UVC/H_2O_2/$TiO_{2(immobilized)}$ systems were investigated. The methods were carried out as recommended by *Standard Methods for the Examination of Water and Wastewater* (APHA 2012).

RESULTS AND DISCUSSION

Aluminum mesh characterization

Structural modifications occurred in the surface of the aluminum-can rings after the calcination step and TiO_2 immobilization (Figure 1).

According to Figure 1(a) and 1(b), it can be seen that the thermal treatment caused an increase in surface roughness, as expected, and in Figure 1(c), a smoother surface is observed when compared with Figure 1(b), indicating titania partially filled the pores of the treated aluminum material.

Figure 2 shows the XRD diffractogram of titania over the aluminum mesh. The qualitative analysis of the crystallographic composition after TiO_2 immobilization identified aluminum presence by the peaks at 43.2°, 44.8° and 78.0° in the support, which is in accordance with the results presented by Ayieko *et al.* (2015).

As can be seen in Figure 2(a), the peaks at $2\theta = 25.5°$ 37.2°, 38.6°, 48.3°, 55.0°, 62.6° and 75.1° represent the anatase phase of TiO_2 while the rutile phase is identified by the peaks at $2\theta = 27.9°$, 41.2°, 54.5°, 65.2° and 69.5° for titania

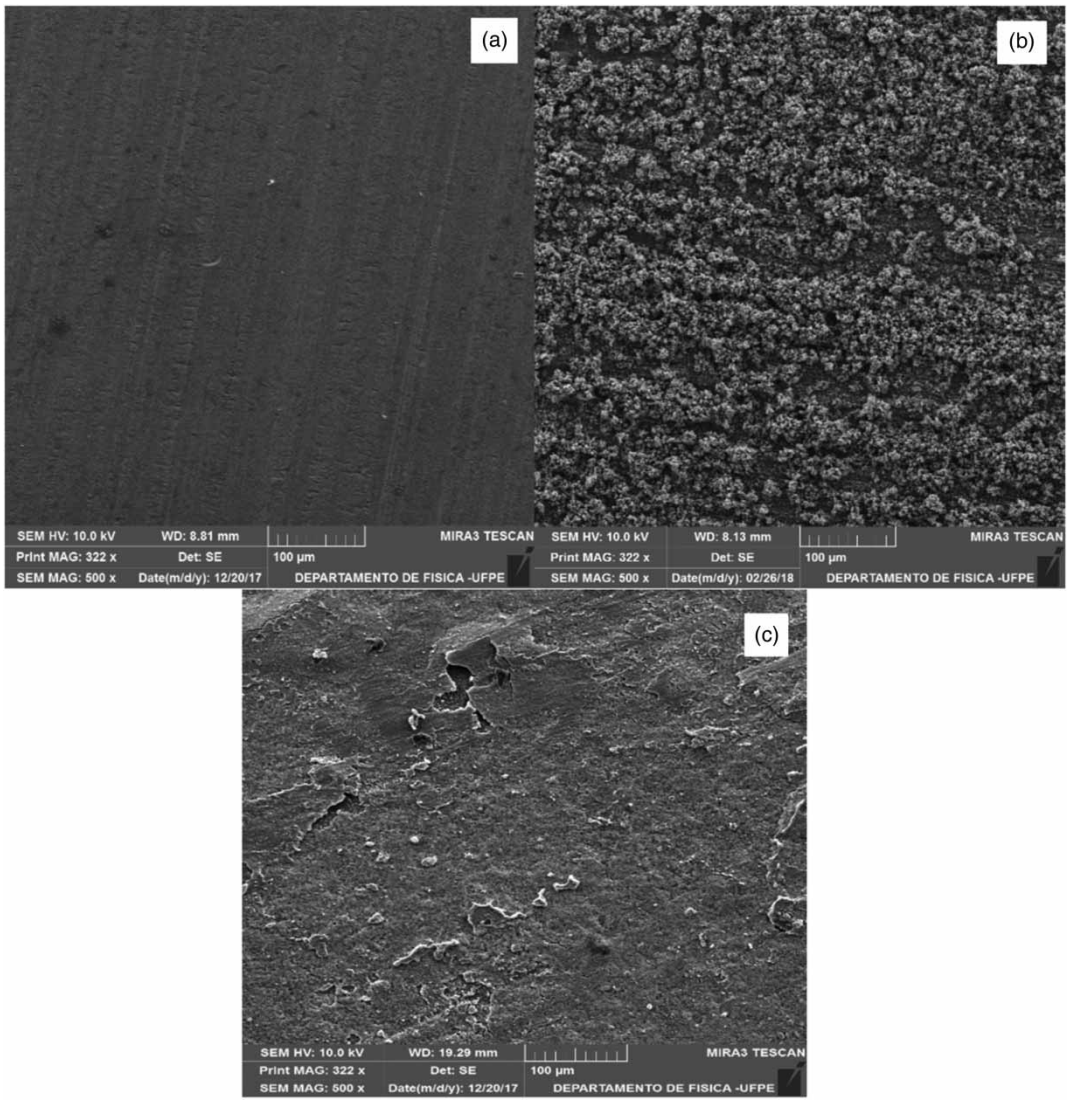

Figure 1 | SEM images of (a) the raw aluminum mesh, (b) calcined aluminum mesh and (c) TiO_2-immobilized aluminum mesh (500×).

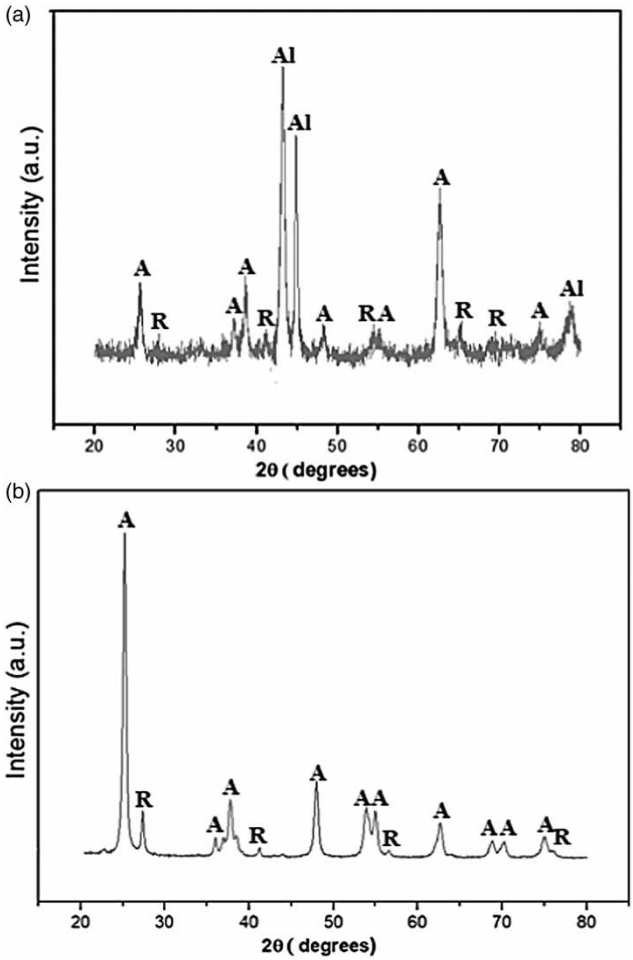

Figure 2 | X-ray diffractogram of (a) titania immobilized over aluminum seals and (b) titania P25 powder (raw photocatalyst). (A – anatase; R – rutile; Al – aluminum.)

crystallographic planes. The content of each crystalline phase of titania was also measured in the aluminum meshes coated with TiO_2-P25 (80% anatase and 20% rutile). The calcined material exhibited a decrease in anatase phase content to 70% after immobilization, which may be associated with the thermal treatment. In Figure 2(b), some of the anatase peaks are observed at 53.8°, 68.7° and 70.2° and they are no longer observed in the calcined titania, some peaks even being replaced by rutile ones. Nadarajan *et al.* (2015) obtained similar results when they evaluated the crystallographic properties of TiO_2 at 500 °C and achieved 70:30 proportion of the anatase and rutile phases, respectively.

Thermal treatment is believed to promote/cause an increase in rutile phase content regarding the commercial TiO_2-P25. The heat treatment is responsible for enhancing roughness, pointed out to be related to amorphous aluminum oxide formation, which enhances the surface area and eases the adherence of powder in the pores (Figure 1(a) and 1(b)). After the immobilization (Figure 1(c)), smaller particles are observed on the mesh's surface in relation to Figure 1(b), indicating that the TiO_2 crystals (Nadarajan *et al.* 2015) are appropriately immobilized on the metallic surface.

Preliminary tests

No considerable degradation rates were achieved in any of the systems run in the absence of UVC radiation. Since favourable degradation rates were achieved in the UVC systems, the breaking of organic molecules is linked to photon absorption rate by the oxidizing agents, promoting the generation of free radicals and electron–hole pairs (Velo-Gala *et al.* 2017).

The UVC system presented the lowest degradation rate achieving only 15.9% after 240 minutes. UVC/$TiO_{2(suspended)}$ and UVC/$TiO_{2(immobilized)}$ systems exhibited 58.3% and 49.2% degradation rates, respectively, while UVC/H_2O_2 exhibited 61.0% for the same photocatalytic reaction time. The most efficient systems were UVC/H_2O_2/$TiO_{2(suspended)}$ and UVC/H_2O_2/$TiO_{2(immobilized)}$, which reached 85.0% and 71.6% degradation, respectively.

UV radiation is able to break organic bonds in complex structures, although, effective mineralization of the pollutants is normally not possible to achieve, even after long operation times. The combined effect of UV and H_2O_2 leads to the formation of highly oxidizing radicals that transform large molecules in smaller structures non-selectively (Raizada *et al.* 2017). Hydrogen peroxide is homolitically broken at $\lambda = 200$–280 nm, which makes feasible the application of UVC radiation to the generation of hydroxyl radicals *in situ* (Jia *et al.* 2018). TiO_2 is photoactivated generating hydroxyl (•OH), superoxide ($\bullet O_2^-$) and hydroperoxide (•OOH) radicals by oxidizing water molecules and being restored at the end of the operation (Wiedmer *et al.* 2016).

A synergistic effect is often observed when H_2O_2 and TiO_2 are employed in photoabsorption and generation of radicals by enhancing the global rate of degradation. H_2O_2 presence is also pointed out to suppress the recombination of electron–holes in the photocatalytic activity of titania, thus, favouring the removal of pollutants from water (Borges *et al.* 2016). Other works have reported similar results (Nascimento Júnior *et al.* 2018; Barbosa *et al.* 2019). In addition to the mass transfer limitations associated with the immobilized system, the decrease of anatase content, as observed in the XRD analysis, may also be responsible

for the lower efficiency of immobilized systems when compared with the usage of titania in suspension.

Experimental planning design

The degradation results varied from 67.18% (in the experiment with the three negative levels) to 96.88% (with higher levels of time and titania concentration), although maximum degradation rates (100%) were attained only at the assay in which the three positive levels were employed ($[TiO_2] = 666.7$ mg·L^{-1}; $[H_2O_2] = 8.20$ mmol·L^{-1}; time = 240 min). The central point was carried out in triplicate and exhibited around 85% degradation rates and the experimental pure error was estimated at 0.071, corroborating the reproducibility of the experiments.

The influence of the parameters and their interaction was investigated statistically. The Pareto chart for the statistical significance of the independent variables is exhibited in Figure 3.

According to the chart, all the independent variables and their interactions exhibited statistical significance. Santos *et al.* (2018) and Barbosa *et al.* (2019) obtained similar results in the degradation of emergent contaminants in heterogeneous photocatalytic systems. The individual independent variables and the interaction among the three proved to influence the degradation rate positively. Thus, the range of time and H_2O_2 and TiO_2 concentrations used to perform this study did not reach an excess and are directly proportional to the degradation rates due to a higher content of free radicals (Nascimento Júnior *et al.* 2018).

Kinetic study of TBEP degradation

From the selected conditions in the experimental design (8.20 mmol·L^{-1} of H_2O_2 and 666.7 mg·L^{-1} of TiO_2), concentration profiles were built for the degradation of TBEP in UVC/H_2O_2/$TiO_{2(suspension)}$ and UVC/H_2O_2/$TiO_{2(immobilized)}$ (Figure 4).

As can be seen in Figure 4, the UVC/H_2O_2/$TiO_{2(suspension)}$ and UVC/H_2O_2/$TiO_{2(immobilized)}$ systems reached removal rates of 97.45% and 71.26%, respectively, after 180 minutes. Complete degradation of TBEP was attained in the TiO_2-suspended system in 240 minutes and in the TiO_2-immobilized system in 360 minutes. The pseudo-first-order kinetic model is pointed out to fit the degradation data of organophosphate esters by AOP processes in other works (Antonopoulou *et al.* 2016; Sharma *et al.* 2016) reporting the degradation of very diluted samples of the flame retardant.

The kinetic rate constants were estimated at $k = 0.0129 \pm 0.0009$ min^{-1} ($R^2 = 0.9716$) and 0.0079 ± 0.0006 min^{-1} ($R^2 = 0.9721$) for the UVC/H_2O_2/$TiO_{2(suspension)}$ and UVC/H_2O_2/$TiO_{2(immobilized)}$ systems, respectively, by the pseudo-first-order model. As a consequence, the half-life reaction time was increased from 53.73 to 87.74 minutes from the TiO_2-suspended to the TiO_2-immobilized system. Antonopoulou *et al.* (2016) found similar results ($k = 0.0141$ min^{-1}) in the degradation of tris(1-chloro-2-propyl) phosphate in TiO_2 heterogeneous photocatalytic systems.

In the estimated residual distributions for the UVC/H_2O_2/$TiO_{2(suspension)}$ and UVC/H_2O_2/$TiO_{2(immobilized)}$ results,

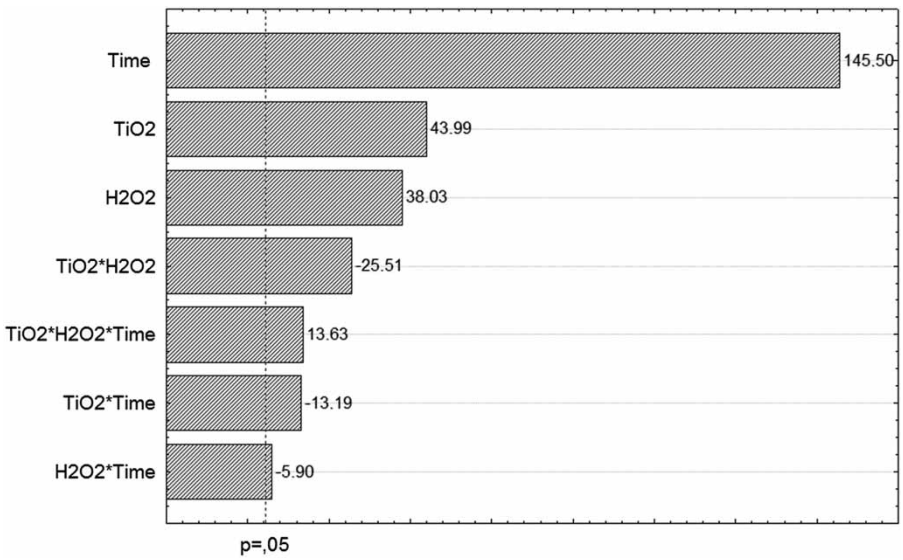

Figure 3 | Pareto chart for the 2^3 experimental design in UVC/H_2O_2/$TiO_{2(suspension)}$.

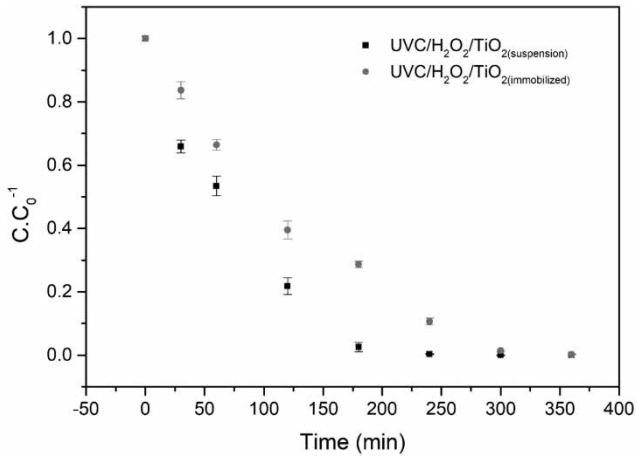

Figure 4 | Concentration profiles of TBEP degradation in $UVC/H_2O_2/TiO_{2(suspension)}$ and $UVC/H_2O_2/TiO_{2(immobilized)}$. $[TiO_2] = 666.7\ mg{\cdot}L^{-1}$, $[H_2O_2] = 8.20\ mmol{\cdot}L^{-1}$.

variances of 0.0134 and 0.0177 were assessed, correspondingly. The low values of variance indicate a good fit of the model to the experimental data along with the R^2 results, similarly to the work reported by Barros Neto *et al.* (2010).

The TiO_2-suspended systems are, in general, able to achieve higher removal rates since they provide higher contact area between the catalyst, the radiation, and the water and pollutant molecules. In TiO_2-immobilized systems, there is a reduction in the photon harvesting rates due to the lower surface area of titania and mass-transfer limitations regarding the TiO_2 suspension samples (Rostami-Vartooni *et al.* 2016). The same effect was observed by Aquino *et al.* (2019) when the efficiency of titania was compared in suspension samples and immobilized over polyethylene terephthalate plates. However, the TiO_2-immobilized systems reduce costs in additional separation steps, which represent an economic advantage. Moreover, the use of a recyclable and low-cost material remodels the process to be more environmentally friendly.

The training of the ANN from the experimental data obtained is exhibited in Figure 5 for both the $UVC/H_2O_2/TiO_{2(suspension)}$ and $UVC/H_2O_2/TiO_{2(immobilized)}$ systems.

From Figure 5(a) and 5(b), the input layers (normalized from −1 to 1) can be seen that represent degradation times and are linked to the output ones, where concentration is calculated at time t (also normalized from −1 to 1). The network multiplies the input values by their respective weights (numbered on the lines that are linked to the neurons), summed to the bias (numbered on the neurons), computed by the sigmoidal activation function between −1 and 1 and finally multiplied by the weights to provide a numeric response.

The pseudocode for the $UVC/H_2O_2/TiO_{2(suspension)}$ is displayed below:

```
//Input normalization
Input = 2*(Input)/360 − 1;
//Computation
Output = 2.283514*(2/(1 + exp(−1*(2.252896*(2/(1 + exp(−1*(−1.872869*Input − 2.2727))) − 1) − 1.136663*(2/(1 + exp(−1*(0.2178829*Input − 1.568911))) − 1) + 0.5732782))) − 1);
//Output denormalization
Output = 0.499*Output + 0.501;
```

For the $UVC/H_2O_2/TiO_{2(immobilized)}$ system the pseudocode is as follows:

```
//Input normalization
Input = 2*Input/360 − 1;
//Computation
Output = 2.848087*(2/(1 + exp(−1*(0.3007855*(2/(1 + exp(−1*(0.6244544*Input − 1.322824))) − 1) − 1.500366*(2/(1 + exp(−1*(2.905448*Input + 2.782597))) − 1) + 0.8577532))) − 1);
//Output denormalization
Output = 0.5*Output + 0.5;
```

From Figure 5(c), it is possible to conclude that the ANN models provided a satisfactory fitting to the experiments. The average error was estimated at 0.0199 for the TiO_2-suspended system and 0.0138 for the TiO_2-immobilized system and R^2 values were estimated at 0.988 and 0.994 for both systems, respectively. Both correlation coefficients are presented to be superior than that obtained by the fitting to the pseudo-first-order kinetic model. Thus, the ANN model is able to predict the degradation rates at a range of conditions with lower deviation than the previous model.

Reuse of aluminum meshes

To evaluate the reuse capacity of the TiO_2–aluminum meshes, cycles of degradation were performed in the same conditions as the kinetic study. In the first three cycles, 100% of TBEP was attained in 360 minutes indicating no significant loss of photocatalytic activity. In the fourth and fifth cycles, TBEP degradation rates reached 99.8% and 98.7% respectively, demonstrating a slight decrease in the activity of the meshes. These results may be associated with the adsorption of byproducts of the degradation on the surface of the titania, occupying active sites and hindering photon absorption (Bel Hadjltaief *et al.* 2016). However, the use of TiO_2–aluminum meshes presents itself as a feasible alternative for reuse in scale-up application since the decrease in photocatalytic activity is minor after five cycles.

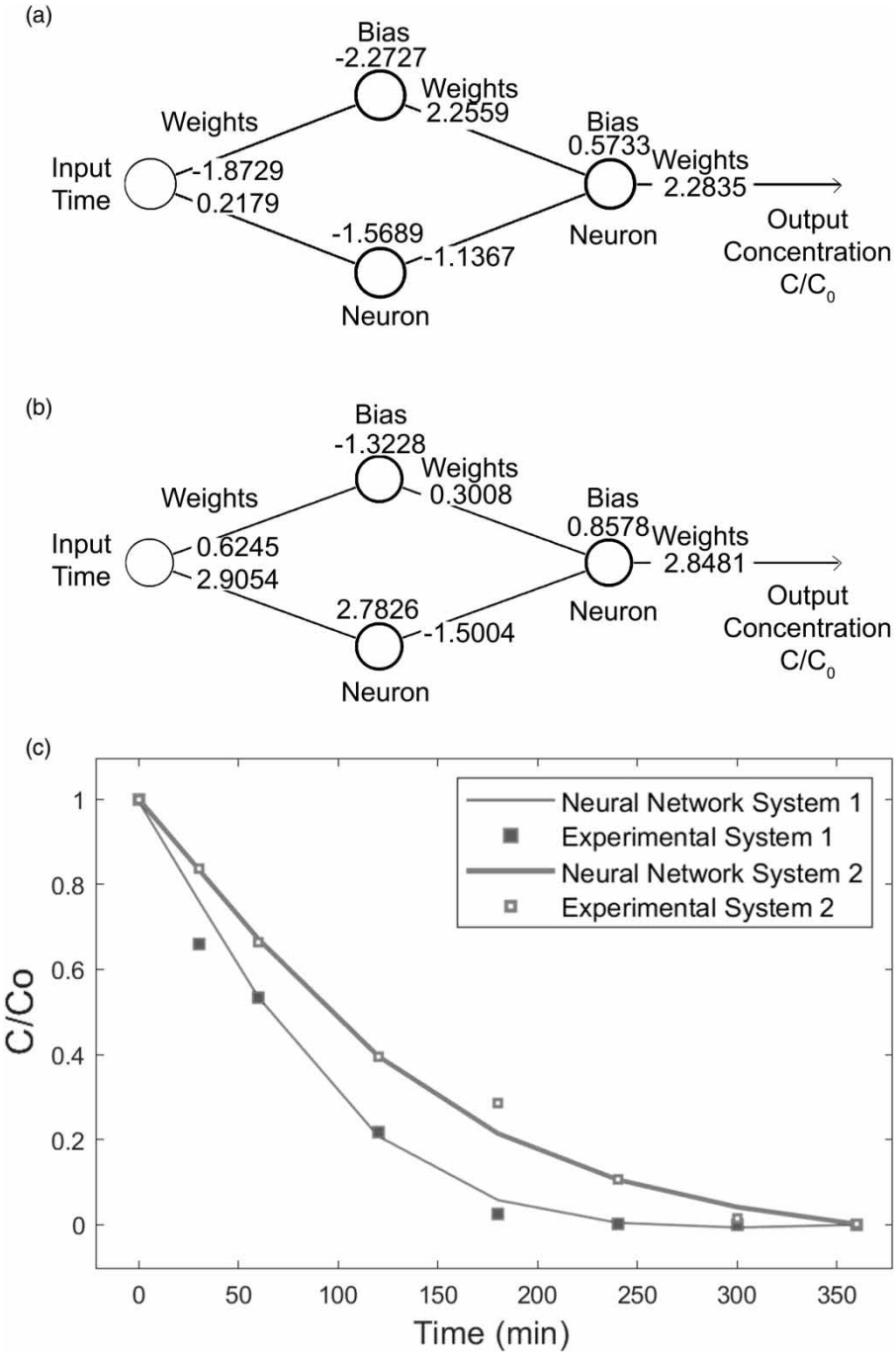

Figure 5 | ANNs applied to the degradation data of TBEP in (a) UVC/H_2O_2/$TiO_{2(suspension)}$, (b) UVC/H_2O_2/$TiO_{2(immobilized)}$ systems and (c) fitting to the experimental data of both systems (1: UVC/H_2O_2/$TiO_{2(suspension)}$ and 2: UVC/H_2O_2/$TiO_{2(immobilized)}$).

Toxicity bioassays and water quality parameters

From the phytotoxicity assay, IC_{50} was estimated for raw and treated TBP samples in the UVC/H_2O_2/$TiO_{2(suspension)}$ and UVC/H_2O_2/$TiO_{2(immobilized)}$ systems. The germination and root growth rates, RGI and IC_{50} are exhibited in Table 1. The root growth and RGI were calculated based on TBEP samples at a concentration of 1.0 mg·L^{-1}.

Since germination rates were higher than 90% in the negative control, the phytotoxicity assay was considered valid (Utzig *et al.* 2019). From Table 1, it is possible to conclude that both photocatalytic treatments led to lower

Table 1 | Phytotoxicity parameters for the raw and treated TBEP samples by AOP systems with *Lactuca sativa* seeds

Sample	Germination rate (%)	Average root growth (cm)	RGI	IC_{50} ($mg \cdot L^{-1}$)
Raw TBEP[a]	90	1.6 ± 0.3	0.69	0.8 ± 0.1
UVC/H_2O_2/$TiO_{2(suspension)}$	97	2.1 ± 0.2	0.91	1.2 ± 0.3
UVC/H_2O_2/$TiO_{2(immobilized)}$	95	1.9 ± 0.1	0.82	1.0 ± 0.3
Negative control[b]	100	2.3 ± 0.3	–	–
Positive control[c]	0	–	–	–

[a]TBEP (1.0 $mg \cdot L^{-1}$).
[b]Distilled water.
[c]Hg_2SO_4 (0.5 $mmol \cdot L^{-1}$).

Table 2 | Water quality parameters for the raw and treated TBEP samples by AOP systems

Sample	COD ($mg \cdot L^{-1}$)	pH	Conductivity ($\mu S \cdot cm^{-1}$)
Raw TBEP	28.07	7.11	3.73
UVC/H_2O_2/$TiO_{2(suspension)}$	5.52	6.62	7.56
UVC/H_2O_2/$TiO_{2(immobilized)}$	9.64	6.11	6.89

acute phytotoxicity levels of the TBEP samples since RGI was considerably magnified. According to the RGI results, lettuce radicles did not demonstrate growth inhibition by the treatment (RGI values > 0.8) while the raw sample demonstrated the existence of inhibitory effects (RGI < 0.8). The IC_{50} index corroborates that byproducts of TBEP photocatalytic removal were not more toxic than the parent compound. A slight increase in its value for both treatment systems indicates the inhibition concentration to 50% of the organisms was higher after treatment. The positive control did not present a considerable germination rate, as expected, and a growth was noticed of 0.3 cm for the UVC/H_2O_2/$TiO_{2(immobilized)}$ and 0.5 cm for the UVC/H_2O_2/$TiO_{2(suspension)}$ system.

Table 2 displays the water quality parameters determined for raw and treated samples after 240 minutes of operation in the UVC/H_2O_2/$TiO_{2(suspension)}$ and UVC/H_2O_2/$TiO_{2(immobilized)}$ systems.

COD values decreased around 80.3% and 65.6% in the AOP systems. The slight decrease in pH after the treatments may be associated with the formation of carbonic acid, often reported in AOP operation (Rayaroth *et al.* 2015). Conductivity is also associated with the byproducts of the degradation since inorganic ions are expected to be formed (Aquino *et al.* 2019). In the case of TBEP mineralization, phosphate anions are expected to remain in the samples after the treatment.

CONCLUSIONS

In conclusion, high rates of degradation were achieved in UVC/H_2O_2/TiO_2 systems employing either suspended or immobilized titania powder for 360 minutes of operation (100% and 98.7%, respectively), even after five cycles for the immobilized titania treatment. From pseudo-first-order kinetic fitting, 0.0129 and 0.0079 min^{-1} were achieved as rate constants for titania in suspension and TiO_2–aluminum mesh AOP systems, respectively. ANN was demonstrated to be a feasible method to describe the experimental data of TBEP degradation. Acute toxicity of the degradation byproducts was demonstrated to be lower for treated samples when compared with raw TBEP solution and along with water quality analyses made TiO_2–aluminum meshes a suitable alternative in the treatment of emergent contaminants to minimize operation costs, besides being environmentally friendly.

REFERENCES

Antonopoulou, M., Karagianni, P. & Konstantinou, I. K. 2016 Kinetic and mechanistic study of photocatalytic degradation of flame retardant tris (1-chloro-2-propyl) phosphate (TCPP). *Applied Catalysis B, Environmental* **192**, 152–160. 10.1016/j.apcatb.2016.03.039.

APHA 2012 *Standard Methods for the Examination of Water and Wastewater*, 22nd edn. American Public Health Association, American Water Works Association, Water Environment Federation, Washington, DC, USA.

Aquino, R. V. S., Barbosa, A. A., Ribeiro, L. B., Oliveira, A. F. B., Silva, J. P., Azoubel, P. M. & Rocha, O. R. S. 2019 Degradation of leaf green food dye by heterogeneous photocatalysis with TiO_2 over a polyethylene terephthalate plate. *Chemical Papers* **73** (10), 2501–2512. https://doi.org/10.1007/s11696-019-00804-y.

Ayieko, C. O., Musembi, R. J., Ogacho, A. A., Aduda, B. O., Muthoka, B. M. & Jain, P. K. 2015 Controlled texturing of aluminum sheet for solar energy applications. *Advances in Materials Physics and Chemistry* **5**, 458–466. http://dx.doi.org/10.4236/ampc.2015.511046.

Barbosa, A. A., de Aquino, R. V. S., Oliveira, A. F. B., Dantas, R. F., Silva, J. P., Duarte, M. M. M. B. & Rocha, O. R. S. 2019 Development of a new photocatalytic reactor built from recyclable material for the treatment of textile industry effluents. *Desalination and Water Treatment* **151**, 82–92. https://doi.org/10.5004/dwt.2019.23905.

Barros Neto, B., Scarminio, I. S. & Bruns, R. E. 2010 *Como Fazer Experimentos: Pesquisa e Desenvolvimento na Ciência e na Indústria (How to Do Experiments: Research and Development in Science and Industry)*, 4th edn. Editora da Unicamp, Campinas, Brazil.

Bayarri, B., Abellán, M. N., Giménez, J. & Esplugas, S. 2007 Study of the wavelength effect in the photolysis and heterogeneous photocatalysis. *Catalysis Today* **129**, 231–239. https://doi.org/10.1016/j.cattod.2007.08.006.

Bel Hadjltaief, H., Ben Zina, M., Galvez, M. E. & Da Costa, P. 2016 Photocatalytic degradation of methyl green dye in aqueous solution over natural clay-supported ZnO–TiO_2 catalysts. *Journal of Photochemistry and Photobiology A: Chemistry* **315**, 25–33. http://dx.doi.org/10.1016/j.jphotochem.2015.09.008.

Borges, S. S., Xavier, L. P. S., Silva, A. C. & Aquino, S. F. 2016 Immobilized titanium dioxide (TiO_2) in different support materials to use in heterogeneous photocatalysis. *Química Nova* **39**, 836–844.

Charamba, L. V. C., Santana, R. M. R., Nascimento, G. E., Charamba, B. V. C., Moura, M. C., Coelho, L. C. B. B., Oliveira, J. G. C., Duarte, M. M. M. B. & Napoleão, D. C. 2018 Application of the advanced oxidative process on the degradation of the green leaf and purple açaí food dyes with kinetic monitoring and artificial neural network modelling. *Water Science and Technology* **78** (5), 1094–1103.

Göb, S., Oliveros, E., Bossmann, S. H., Braun, A. M., Guardani, R. & Nascimento, C. A. O. 1999 Modeling the kinetics of a photochemical water treatment process by means of artificial neural networks. *Chemical Engineering and Processing: Process Intensification* **38**, 373–382. https://doi.org/10.1016/S0255-2701(99)00028-8.

Greaves, A. K., Letcher, R. J., Chen, D., McGoldrick, D. J., Gauthier, L. T. & Backus, S. M. 2016 Retrospective analysis of organophosphate flame retardants in herring gull eggs and relation to the aquatic food web in the Laurentian Great Lakes of North America. *Environmental Research* **150**, 255–263. http://dx.doi.org/10.1016/j.envres.2016.06.006.

Huang, K., Grumezescu, A. M., Chang, C., Yang, C. & Wang, C. 2014 Immobilization and stabilization of TiO_2 nanoparticles in alkaline-solidificated chitosan spheres without cross-linking agent. *International Journal of Latest Research in Science and Technology* **3** (2), 174–178.

Jia, P., Zhou, Y., Zhang, X., Zhang, Y. & Dai, R. 2018 Cyanobacterium removal and control of algal organic matter (AOM) release by UV/H_2O_2 pre-oxidation enhanced Fe(II) coagulation. *Water Research* **131**, 122–130. https://doi.org/10.1016/j.watres.2017.12.020.

Nadarajan, R., Bakar, W. A. W. A. & Ali, R. 2015 Effect of calcination temperature on metal oxides and their photocatalytic activity. *Advanced Materials Research* **1107**, 73–78.

Nascimento Júnior, W. J. D., da Rocha, O. R. S., Dantas, R. F., da Silva, J. P. & Barbosa, A. A. 2018 Kinetic study of food dyes removal from aqueous solutions by solar heterogeneous photocatalysis with artificial neural networks and phytotoxicity assessment. *Desalination and Water Treatment* **104**, 304–314.

Nasirian, M., Bustillo-Lecompte, C. F. & Mehrvar, M. 2017 Photocatalytic efficiency of Fe_2O_3/TiO_2 for the degradation of typical dyes in textile industries: effects of calcination temperature and UV-assisted thermal synthesis. *Journal of Environmental Management* **196**, 487–498. http://dx.doi.org/10.1016/j.jenvman.2017.03.030.

Raizada, P., Shandilya, P., Singh, P. & Thakur, P. 2017 Solar light-facilitated oxytetracycline removal from the aqueous phase utilizing a H_2O_2/$ZnWO_4$/CaO catalytic system. *Journal of Taibah University for Science* **11** (5), 689–699. http://dx.doi.org/10.1016/j.jtusci.2016.06.004.

Rayaroth, M. P., Aravind, U. K. & Aravindakumar, C. T. 2015 Sonochemical degradation of Coomassie Brilliant Blue: effect of frequency, power density, pH and various additives. *Chemosphere* **119**, 848–855. http://dx.doi.org/10.1016/j.chemosphere.2014.08.037.

Rostami-Vartooni, A., Nasrollahzadeh, M., Salavati-Niasari, M. & Atarod, M. 2016 Photocatalytic degradation of azo dyes by titanium dioxide supported silver nanoparticles prepared by a green method using *Carpobrotus acinaciformis* extract. *Journal of Alloys and Compounds* **689**, 15–20. http://dx.doi.org/10.1016/j.jallcom.2016.07.253.

Santos, M. M. M., Duarte, M. M. M. B., Nascimento, G. E., Souza, N. B. G. & Rocha, O. R. S. 2018 Use of TiO_2 photocatalyst supported on residues of polystyrene packaging and its applicability on the removal of food dyes. *Environmental Technology* **40** (12), 1494–1507. https://doi.org/10.1080/09593330.2017.1423396.

Sharma, A. K., Tiwari, R. K. & Gaur, M. S. 2016 Nanophotocatalytic UV degradation system for organophosphorus pesticides in water samples and analysis by Kubista model. *Arabian Journal of Chemistry* **9**, S1755–S1764. http://dx.doi.org/10.1016/j.arabjc.2012.04.044.

Utzig, L. M., Lima, R. M., Gomes, M. F., Ramsdorf, W. A., Martins, L. R. R., Liz, M. V. & Freitas, A. M. 2019 Ecotoxicity response of chlorpyrifos in *Aedes aegypti* larvae and *Lactuca sativa* seeds after UV/H_2O_2 and UVC oxidation. *Ecotoxicology and Environmental Safety* **169**, 449–456. https://doi.org/10.1016/j.ecoenv.2018.11.003.

Velo-Gala, I., Pirán-Montaño, J. A., Rivera-Utrilla, J., Sánchez-Polo, M. & Mota, A. J. 2017 Advanced oxidation processes based on the use of UVC and simulated solar radiation to remove the antibiotic tinidazole from water. *Chemical Engineering Journal* **323**, 605–617. http://dx.doi.org/10.1016/j.cej.2017.04.102.

Veréb, G., Ambrus, Z., Pap, Z., Mogyorósi, K., Dombi, A. & Hernádi, K. 2014 Immobilization of crystallized photocatalysts on ceramic paper by titanium(IV) ethoxide and photocatalytic decomposition of phenol. *Reaction Kinetics, Mechanisms and Catalysis* **113**, 293–303. https://doi.org/10.1007/s11144-014-0734-y.

Verran, G. O., Kurzawa, U. & Pescador, W. A. 2005 Reciclagem de latas de alumínio visando melhor rendimento e qualidade metalúrgica no alumínio obtido (Recycling of aluminum cans aiming at better efficiency and metallurgical quality in the obtained aluminum). *Revista Matéria* **10** (1), 72–79.

Vykoukalová, M., Venier, M., Vojta, Š., Melymuk, L., Bečanová, J., Romanak, K., Prokeš, R., Okeme, J. O., Saini, A., Diamond, M. L. & Klánová, J. 2017 Organophosphate esters flame

retardants in the indoor environment. *Environment International* **106**, 97–104. https://doi.org/10.1016/j.envint.2017.05.020.

Wiedmer, D., Sagstuen, E., Welch, K., Haugen, H. J. & Tiainen, H. 2016 Environmental oxidative power of aqueous non-irradiated TiO_2-H_2O_2 suspensions: methylene blue degradation and the role of reactive oxygen species. *Applied Catalysis B: Environmental* **198**, 9–15. http://dx.doi.org/10.1016/j.apcatb.2016.05.036.

Xing, X., Du, Z., Zhuang, J. & Wang, D. 2018 Removal of ciprofloxacin from water by nitrogen doped TiO_2 immobilized on glass spheres: rapid screening of degradation products. *Journal of Photochemistry and Photobiology A: Chemistry* **359**, 23–32. https://doi.org/10.1016/j.jphotochem.2018.03.026.

First received 9 May 2019; accepted in revised form 20 October 2019. Available online 31 October 2019